

## Supporting Information

### Preparation and Characterization of Novel Ag doped Hydroxyapatite-Fe<sub>3</sub>O<sub>4</sub>-Chitosan hybrid composites and its In vitro Biological evaluations for Orthopaedic applications

U. Anjaneyulu<sup>a</sup>, V.K. Swaroop<sup>b</sup> and U. Vijayalakshmi<sup>a\*</sup>

<sup>a</sup>Materials Chemistry Division, School of Advanced Sciences, VIT University

<sup>b</sup>Biomedical Science Division, School of Biosciences and Technology, VIT University

Vellore -632014. Tamil Nadu, India.

Tel: +91-416-2202464; Fax: +91-416-224 3092.

E-mail address: [vijayalakshmi.u@vit.ac.in](mailto:vijayalakshmi.u@vit.ac.in), [lakesminat@yahoo.com](mailto:lakesminat@yahoo.com)

**Fig. S1** ATR-FTIR spectroscopy of Sol-Gel synthesized silver doped HAP sintered at 900 °C for 2 h (a) 1%, (b) 3% and (c) 5%.

**Fig. S2** Powder-XRD patterns of Sol-Gel synthesized silver doped HAP sintered at 900 °C for 2 h (a) 1%, (b) 3% and (c) 5%.

**Fig. S3** Antibacterial activity by colony count method against E.coli and S.aureus of 10<sup>-3</sup> control (1a&b), 1%@Ag:HAP (2a&b), 3%@Ag:HAP (3a&b), 5%@Ag:HAP (4a&b), Fe<sub>3</sub>O<sub>4</sub> (5a&b), C-1 (6a&b), C-2 (7a&b) and C-3 (8a&b).

**Fig. S4** Release of Ag from 5%@Ag:HAP, C-1, C-2 and C-3 powders in PBS solution

**Fig. S5** Photographs of RBC lysis of C-1, C-2 and C-3 hybrid composites at different concentrations 200 µg/ml (a), 400 µg/ml (b), 600 µg/ml (c), 800 µg/ml (d) and 1000 µg/ml (e).

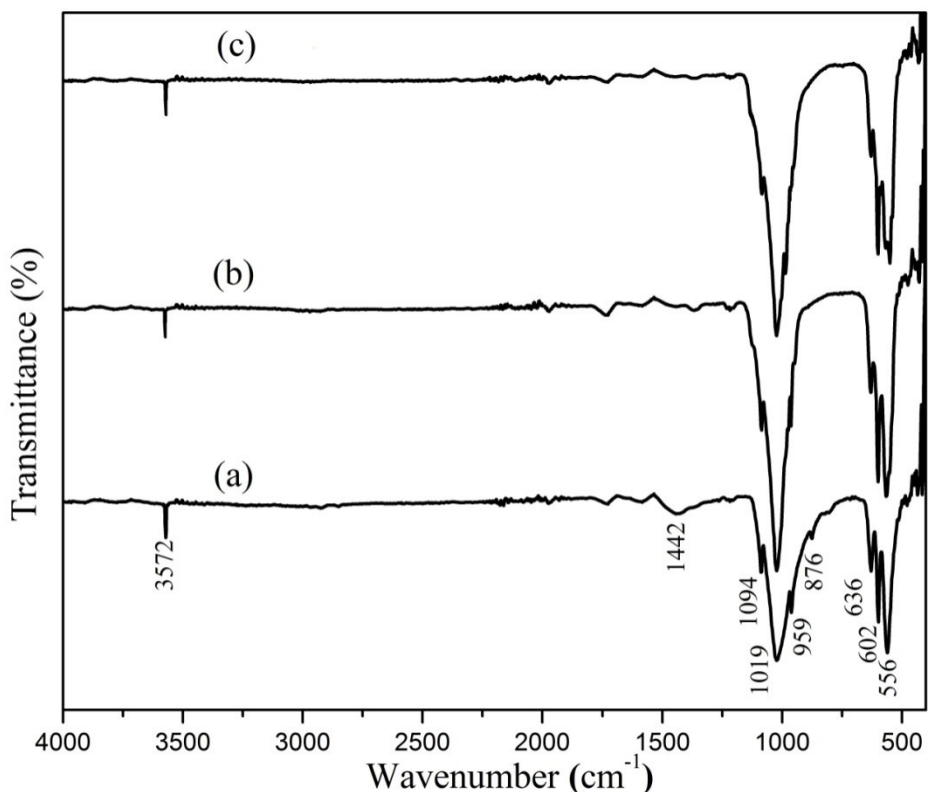


**Fig. S1** ATR-FTIR spectroscopy of Sol-Gel synthesized silver doped HAP sintered at 900 °C for 2 h (a) 1%, (b) 3% and (c) 5%.

From Fig. S1(a)-(c), it was observed that the bands at 636 and 3572  $\text{cm}^{-1}$  are significant peaks for the stretching and bending mode of the  $\text{OH}^-$  group in the structure of HAP crystal<sup>28</sup>. The intensity of the  $\text{OH}^-$  band at 636  $\text{cm}^{-1}$  was found to be decreased with an increase in the Ag doping concentration from 1 to 5%. The signature of HAP absorption bands at 556-602, 959 and 1019-1094  $\text{cm}^{-1}$  corresponds to bending mode of the O-P-O ( $\nu$  4) bond, symmetrical stretching mode of the P-O ( $\nu$  1) bond and asymmetrical stretching vibrational mode of the P-O ( $\nu$ 3) bond in phosphate group are observed in all the concentrations<sup>29</sup>. The doublet peaks of  $\text{PO}_4^{3-}$  moiety at 556-602 and 1019-1094  $\text{cm}^{-1}$  are highly evident for the formation of crystalline HAP. It was found that the peak intensity of  $\text{PO}_4^{3-}$  group at 959  $\text{cm}^{-1}$  was minimized with increase in the Ag concentration. The sharp and broad peaks at 876 and 1442  $\text{cm}^{-1}$  denotes the presence of carbonate ( $\text{CO}_3^{2-}$ ) ions which are involved in the replacement of  $\text{PO}_4^{3-}$  ions in the apatite structure (B-type apatite). The  $\text{CO}_3^{2-}$  bands are gradually disappeared with an increase in the doping concentration of Ag in HAP system. The reduction in the peak intensities of  $\text{OH}^-$ ,  $\text{PO}_4^{3-}$  and  $\text{CO}_3^{2-}$  indicates the slight alteration of HAP structure and this was further proved by powder-XRD analysis.

The FTIR spectrum (Fig. 1 (a)) of pure chitosan shows the significant absorption peaks at 882 and 1155  $\text{cm}^{-1}$  which correspond to the C-O linkage of saccharide structure of glucosamine ring. The broad peak assigned at 1019  $\text{cm}^{-1}$  corresponds to stretching vibration of C-O-C bond in the chitosan. The vibrational bands at 2877 and 3329  $\text{cm}^{-1}$  are due to a typical vibration of C-H and symmetrical stretching of N-H bonds in the chitosan.

In C-3 additionally very weak bands were observed in the range of 1315-1654  $\text{cm}^{-1}$  due to existence of CS in the composites, whereas no significant bands for C-1 and C-2 because of the lesser amount CS.

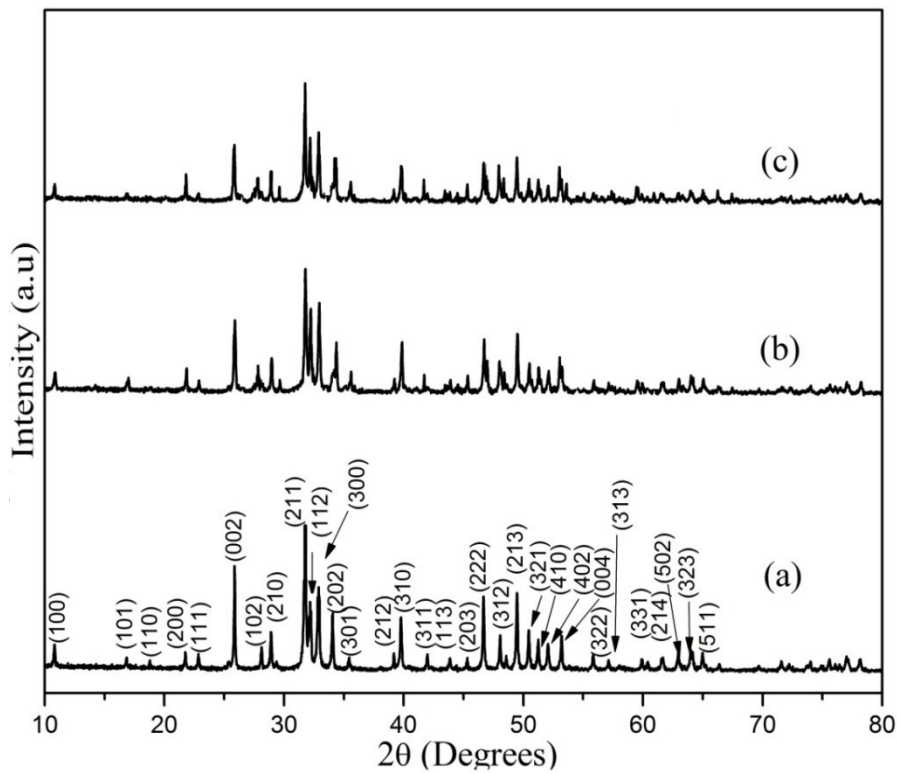


**Fig. S2** Powder-XRD patterns of Sol-Gel synthesized silver doped HAP sintered at 900 °C for 2 h (a) 1%, (b) 3% and (c) 5%.

From this XRD pattern, phase pure Ag doped HAP was formed without any other secondary phases such as  $\beta$ -TCP and metallic silver nanoparticles. Ag concentration increases from 1 to 5%, which leads to change the peak intensities ( $25.75$  to  $34.02^\circ$ ) and cause the reduction in the crystallinity of Ag doped HAP. The lattice parameters of Ag doped HAP increased with an increase in the Ag concentration which might be due to the  $\text{Ag}^+$  (0.128 nm) substituting for  $\text{Ca}^{2+}$  (0.099 nm) in HAP lattice and also one of the major parameter for an increase in the lattice parameters is the ionic radius of  $\text{Ag}^+$  ion larger than the  $\text{Ca}^{2+}$  ion.

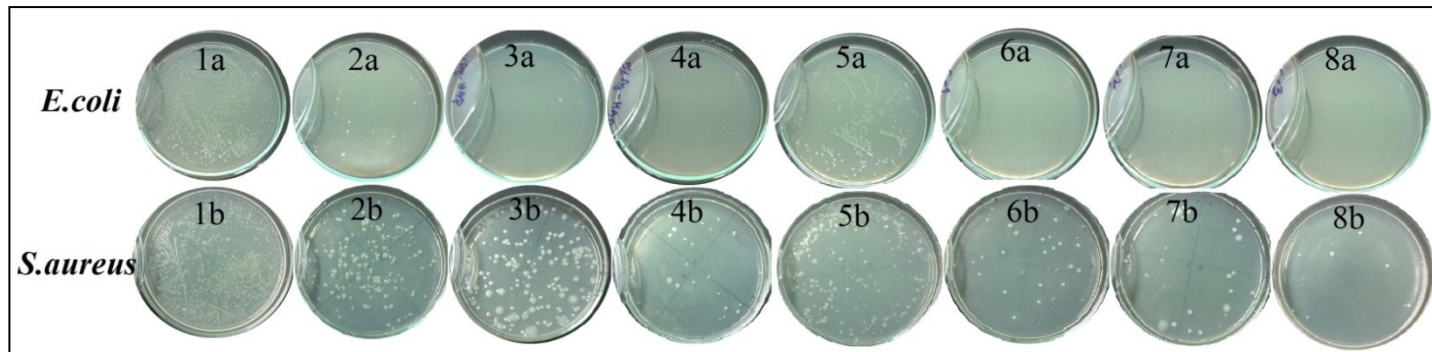


**Fig. S3** Antibacterial activity by colony count method against *E.coli* and *S.aureus* of  $10^{-3}$  control (1a&b), 1%@Ag:HAP (2a&b), 3%@Ag:HAP (3a&b), 5%@Ag:HAP (4a&b),  $Fe_3O_4$  (5a&b), C-1 (6a&b), C-2 (7a&b) and C-3 (8a&b).

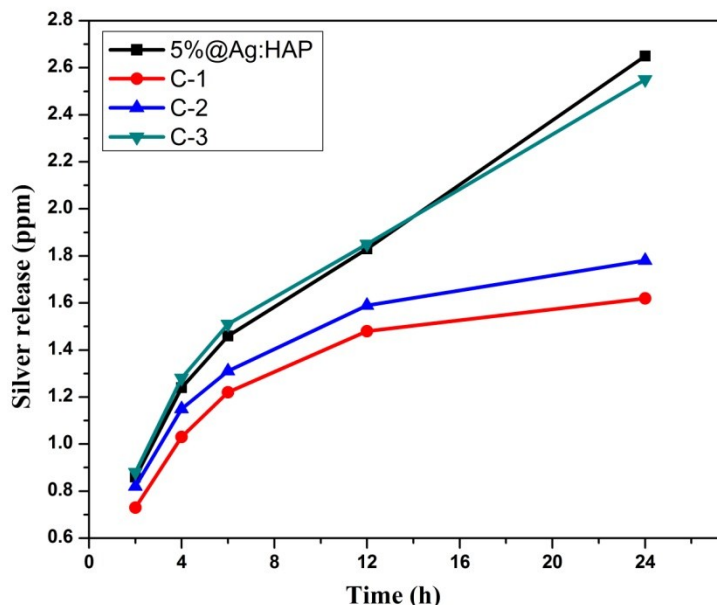


**Fig. S4** Release of Ag from 5%@Ag:HAP, C-1, C-2 and C-3 powders in PBS solution

The silver release study was performed on the 5%@Ag:HAP, C-1, C-2 and C-3 composites in PBS solution with respect to time (Fig. S3). The 5%Ag:HAP and C-3 materials are showed the high amount of Ag released into PBS solution gradually than the C-1 and C-2 at various hours (from 2 to 24 h). The Ag release for 5%Ag:HAP, C-3 are 2.65 and 2.54 ppm whereas C-1, C-2 as 1.62 and 1.78 ppm respectively at the time of 24 h. Hence, 5%Ag:HAP and C-3 material exhibits the excellent inhibition of active growth of *S. aureus* and *E. coli* than the C-1 and C-2 composites.

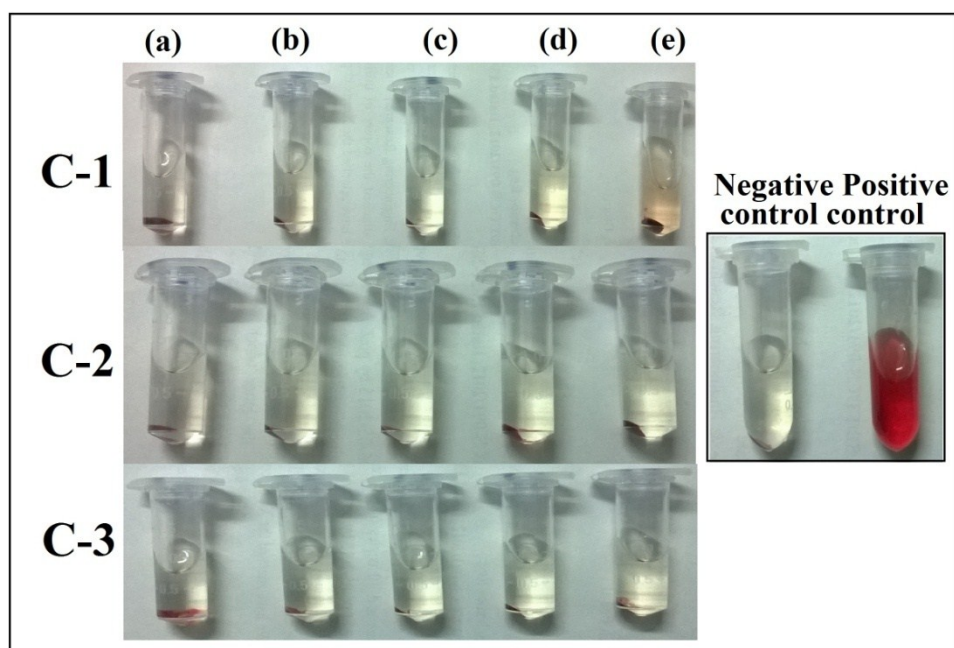


**Fig. S5** Photographs of RBC lysis of C-1, C-2 and C-3 hybrid composites at different concentrations 200 µg/ml (a), 400 µg/ml (b), 600 µg/ml (c), 800 µg/ml (d) and 1000 µg/ml (e).

**Table S1** Calculation of crystallite, crystallinity and lattice parameters of Ag doped HAP.

S. No	Concentration Ag doped HAP	Crystallite Size (D)	Crystallinity (Xc)	Lattice Parameters		Volume (Å <sup>3</sup> )
				a-axis (002) Å	c-axis (300) Å	
1	0.01 M (1%)	44 nm	2.73025	9.4240	6.8611	528.06
2	0.03 M (3%)	50 nm	2.71374	9.4465	6.8753	531.68
3	0.05 M (5%)	67 nm	2.69772	9.4650	6.8858	534.58